RSC Advances

PAPER

View Article Online
View Journal | View Issue

Cite this: *RSC Adv.*, 2017, **7**, 4611

Efficient dye-sensitized solar cells with [copper(6,6′-dimethyl-2,2′-bipyridine)$_2$]$^{2+/1+}$ redox shuttle†

Jiajia Li,‡[a] Xichuan Yang,‡*[a] Ze Yu,[a] Gagik G. Gurzadyan,[a] Ming Cheng,[b] Fuguo Zhang,[a] Jiayan Cong,[c] Weihan Wang,[a] Haoxin Wang,[a] Xiaoxin Li,[a] Lars Kloo,[c] Mei Wang[a] and Licheng Sun[ab]

Received 23rd October 2016
Accepted 13th December 2016

DOI: 10.1039/c6ra25676g

www.rsc.org/advances

The [copper(6,6′-dimethyl-2,2′-bipyridine)$_2$]$^{2+/1+}$ ([Cu(dmbp)$_2$]$^{2+/1+}$) redox couple, which possesses a distorted tetragonal geometry of a Cu(I) complex crystal and a distorted tetrahedral coordination geometry of Cu(II) complex crystal, has been developed as a redox mediator in dye-sensitized solar cells (DSSCs). The energy of loss for dye regeneration was reduced with a very low but sufficient driving force of only 0.11 eV. A distinct increase in open-circuit voltage (V_{OC}) was achieved and a remarkable power conversion efficiency of 10.3% was afforded at 100 mW cm^{-2} under AM 1.5G condition.

The development of abundant and freely accessible solar energy is one of the promising approaches to alleviate energy crisis. As a kind of prospective next-generation photovoltaic device, dye-sensitized solar cells (DSSCs) have attracted worldwide research attention during the past two decades.[1,2] However, energy losses, such as inappropriate electron transfer, the loss-in-overpotential, and the resistive losses, limit the performance of DSSCs.[3] Among these energy losses, the loss-in-overpotential is the main limitation in the high-performance DSSCs, which contains two main sources of electron injection into the metal oxide and the dye regeneration. DSSCs with triiodide/iodide (I_3^-/I^-) system have gained a series of promising results.[4–6] However, the large loss of energy caused by the low redox potential of I_3^-/I^- and the two-step mechanism in the dye regeneration results in a low photovoltage.[7] Development of new shuttles with higher redox potentials is of high importance, particularly, when they act in the one-step regeneration of the oxidation state of dye. It is expected that they may reduce the energy loss to enhance the overall power conversion efficiency (PCE) of DSSCs. Using this strategy, many redox mediators have been introduced into the DSSCs,[8–14] among which the cobalt complex redox systems with the highest efficiencies exceeding 13% should be pointed out.[9,15–17] However, the cobalt-complex redox systems are yet suffering from the limitations of mass-transport and recombination. Moreover, a driving force of more than 0.2 eV for dye regeneration is still required for the high performance DSSCs.[10,18,19]

There have been a few examples that have applied copper-complex redox couples in DSSCs, which mainly focused on the distorted tetragonal geometry architectonic redox couple of [(2,9-dimethyl-1,10-phenanthroline)$_2$copper]$^{2+/1+}$ ([Cu(dmp)$_2$]$^{2+/1+}$).[20,21] Freitag and coworkers demonstrated that a low driving force of only 0.2 eV was sufficient for the device with [Cu(dmp)$_2$]$^{2+/1+}$ as a redox shuttle, and a PCE of 8.3% was achieved in combination with an organic dye **LEG4**.[22] Although the use of a copper-complex-based electrolyte could lead to a relatively high PCE, very few new efficient copper-complex redox systems have been developed.[23] Very recently, Cong and coworkers reported a new copper-complex redox shuttle with bis(1,1-bis(2-pyridyl)ethane) copper(I/II), which yielded an overall efficiency of 9.0%.[24] However, the open-circuit voltage (V_{OC}) was not as high as that of the [Cu(dmp)$_2$]$^{2+/1+}$ device due to the relatively low redox potential. Herein, we introduced a copper-complex redox shuttle with [copper(6,6′-dimethyl-2,2′-bipyridine)$_2$]$^{2+/1+}$ ([Cu(dmbp)$_2$]$^{2+/1+}$,

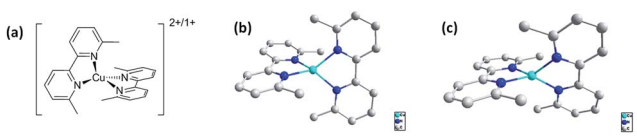

Fig. 1 (a) Molecular structure of [Cu(dmbp)$_2$]$^{2+/1+}$ (b) crystal structure of Cu(dmbp)$_2^+$. (c) Crystal structure of Cu(dmbp)$_2^{2+}$.

[a]State Key Laboratory of Fine Chemicals, Institute of Artificial Photosynthesis, DUT-KTH Joint Education and Research Center on Molecular Devices, Dalian University of Technology (DUT), Dalian 116024, China. E-mail: yangxc@dlut.edu.cn
[b]Organic Chemistry, Center of Molecular Devices, Department of Chemistry, School of Chemical Science and Engineering, KTH Royal Institute of Technology, Teknikringen 30, SE-10044, Stockholm, Sweden
[c]Applied Physical Chemistry, School of Chemical Science and Engineering, Department of Chemistry KTH Royal Institute of Technology, Teknikringen 30, SE-100 44 Stockholm, Sweden

† Electronic supplementary information (ESI) available. CCDC 1511217. For ESI and crystallographic data in CIF or other electronic format see DOI: 10.1039/c6ra25676g

‡ These authors contributed equally to this work.

Fig. 1(a)) into the DSSCs. This copper-based redox system exhibited an extremely small driving force of only 0.11 eV for the regeneration of the oxidized form of the organic sensitizer **Y123** (Fig. 3(b)), but with a quite rapid regeneration. The device based on $[Cu(dmbp)_2]^{2+/1+}$ yielded a sufficiently high V_{OC} of 1048 mV and at the same time, a considerable short-circuit photocurrent density (J_{SC}) of 14.4 mA cm^{-2}, which led to a remarkable PCE of 10.3% at 100 mW cm^{-2} under AM 1.5G conditions.

The details of the synthesis of copper(6,6′-dimethyl-2,2′-bipyridine)$_2$BF$_4$ and copper(6,6′-dimethyl-2,2′-bipyridine)$_2$(BF$_4$)$_2$ complexes are included in the ESI.† The crystal structures of Cu(dmbp)$_2^+$ and Cu(dmbp)$_2^{2+}$ are shown in Fig. 1(b) and (c), respectively. The Cu(dmbp)$_2^+$ complex crystallizes in a distorted tetrahedral geometry with an 80.9° dihedral angle determined by the copper center and each set of nitrogen atoms of 6,6′-dimethyl-2,2′-bipyridine. Cu(dmbp)$_2^{2+}$ complex exhibits a distorted tetrahedral coordination geometry with a dihedral angle of 62.6°. For copper-complexes, internal reorganizational energies are crucial in the electron-transfer behavior upon the twisting of the bond angles. However, for [copper(6,6′-dimethyl-2,2′-bipyridine)$_2$]$^{2+/1+}$, the stacking interaction between the adjacent aromatic ligands leads to a small change in the structure between copper(I) and copper(II) complexes, which is expected to contribute to a very rapid electron self-exchange. Note that according to studies, in this system, the reduction process is relatively slow as compared to the oxidation process.[25]

Considering the low solubility of Cu(dmbp)$_2$BF$_4$, the composition of 0.10 M Cu(dmbp)$_2$BF$_4$, 0.05 M Cu(dmbp)$_2$(BF$_4$)$_2$, 0.50 M 4-*tert*-butylpyridine (TBP), and 0.10 M LiBF$_4$ in acetonitrile was selected. The electrolytes with the I_3^-/I^- and $[Co(bpy)_3]^{3+/2+}$ redox shuttle were composed for comparison. The iodine-based electrolyte contained 0.60 M 1,2-dimethyl-3-propylimidazolium iodide (DMPII), 0.02 M I_2, 0.06 M LiI, and 0.40 M TBP in acetonitrile. The cobalt complex-based electrolyte was composed of 0.22 M Co(bpy)$_3$(ClO$_4$)$_2$, 0.05 M Co(bpy)$_3$(ClO$_4$)$_3$, 0.10 M LiClO$_4$, and 0.50 M TBP in acetonitrile, as previously reported.[26] The DSSCs with the metal-complex based electrolyte were fabricated with a double-layered TiO_2 film of 5.6 μm + 4 μm, whereas a 7.4 μm + 4 μm double-layered TiO_2 film was applied to the devices with I_3^-/I^- system. The organic dye **Y123** was used as the photosensitizer. Other details of solar cell fabrication can be found in the ESI.†

Photocurrent density–voltage (*J*–*V*) characteristics of DSSCs were determined using a working area of 0.126 cm^2 by a mask at 100 mW cm^{-2} under AM 1.5G conditions, as illustrated in Fig. 2(a). The corresponding photovoltaic parameters are presented in Table 1. The DSSC device with the $[Cu(dmbp)_2]^{2+/1+}$-based electrolyte exhibited a J_{SC} of 14.4 mA cm^{-2}, an V_{OC} of 1048 mV, and a fill factor (FF) of 68.1%, resulting in an impressive PCE of 10.3%. The device based on I_3^-/I^- shows a much lower V_{OC} of 724 mV, a higher J_{SC} of 15.8 mA cm^{-2}, and a FF of 70.2%, thus exhibiting a lower PCE of only 8.0%. For the $[Co(bpy)_3]^{3+/2+}$ system, an in-between performance of PCE = 9.2% was obtained with a J_{SC} of 15.3 mA cm^{-2}, a V_{OC} of 844 mV, and a FF of 71.2%. Apparently, the high V_{OC} makes a significant contribution to the outstanding overall conversion efficiency of the $[Cu(dmbp)_2]^{2+/1+}$ system in three redox systems.

The V_{OC} of the DSSCs devices could be described as shown in eqn (1):

$$V_{OC} = E_{red} - E_{CB} - \frac{\gamma k_B T}{e} \ln\left(\frac{N_{CB}}{n_c}\right) \quad (1)$$

where E_{CB} is the conduction band edge of TiO_2, which would be shifted with the change in the chemical circumstance surrounding TiO_2 nanoparticles by alternating the redox systems, E_{red} is the redox potential of the redox shuttle in the electrolyte, γ is a characteristic constant of TiO_2 tailing states, k_B is the Boltzmann constant, T is the temperature, e is the elementary charge, N_{CB} is the effective density of states at the TiO_2 conduction band, and n_C is the number of photoelectrons in TiO_2, which is closely connected to the charge recombination process. According to eqn (1), the V_{OC} mainly depends on $E_{red} - E_{CB}$ and n_C at certain temperatures. The redox potential of $[Cu(dmbp)_2]^{2+/1+}$ from the cyclic voltammetry measurements (Fig. 3(b)) was determined to be 0.97 V *vs.* NHE, which is 0.62 V and 0.41 V more positive than the redox potential of I_3^-/I^- (0.35 V *vs.* NHE) and $[Co(bpy)_3]^{3+/2+}$ (0.56 V *vs.* NHE), respectively (Fig. 3(a)). However, the corresponding V_{OC} enhancement of the $[Cu(dmbp)_2]^{2+/1+}$-based device was 324 mV and 204 mV to the I_3^-/I^- and $[Co(bpy)_3]^{3+/2+}$ system, respectively, which can be ascribed to the synergy of recombination and shifts of the conduction band. Note that the driving force for dye

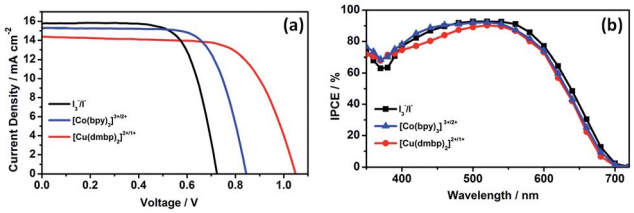

Fig. 2 *J*–*V* curves (a) and IPCE spectra (b) of the DSSCs based on the I_3^-/I^-, $[Co(bpy)_3]^{3+/2+}$, and $[Cu(dmbp)_2]^{2+/1+}$ systems.

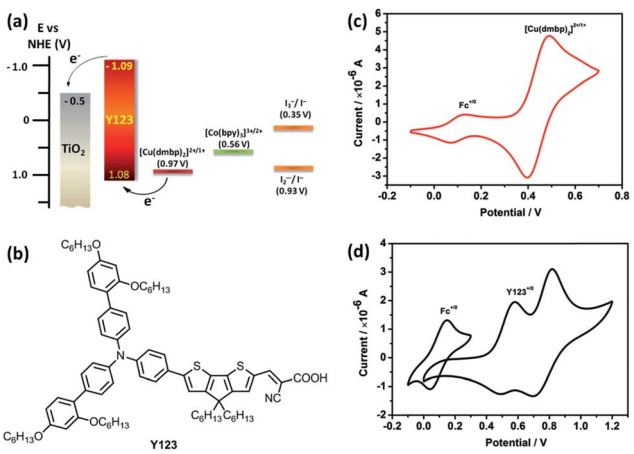

Fig. 3 (a) Schematic for the **Y123** sensitized TiO_2 film with I_3^-/I^-, $[Co(bpy)_3]^{3+/2+}$, and $[Cu(dmbp)_2]^{2+/1+}$ redox systems. (b) Molecular structure of the organic dye **Y123**. (c) Cyclic voltammetry of the Cu(dmbp)$_2^+$ complex. (d) Cyclic voltammetry of the organic dye **Y123** absorbed on the TiO_2 film.

Table 1 Photovoltaic parameters of the DSSCs based on the I_3^-/I^-, $[Co(bpy)_3]^{3+/2+}$, and $[Cu(dmbp)_2]^{2+/1+}$ systems[a]

Electrolyte	J_{SC} (mA cm^{-2})	V_{OC} (mV)	FF (%)	PCE (%)
I_3^-/I^- [b]	15.8 ± 0.3	724 ± 10	70.4 ± 0.6	8.0 ± 0.2
$[Co(bpy)_3]^{3+/2+}$ [c]	15.3 ± 0.3	844 ± 5	71.2 ± 0.7	9.2 ± 0.1
$[Cu(dmbp)_2]^{2+/1+}$ [c]	14.4 ± 0.2	1048 ± 7	68.1 ± 0.5	10.3 ± 0.1

[a] Working area of DSSCs was 0.126 cm^2 under 100 mW cm^{-2} (AM 1.5) conditions. [b] DSSCs were assembled with a double-layered TiO_2 film of 7.4 μm + 4 μm. [c] DSSCs were assembled with a double-layered TiO_2 film of 5.6 μm + 4 μm.

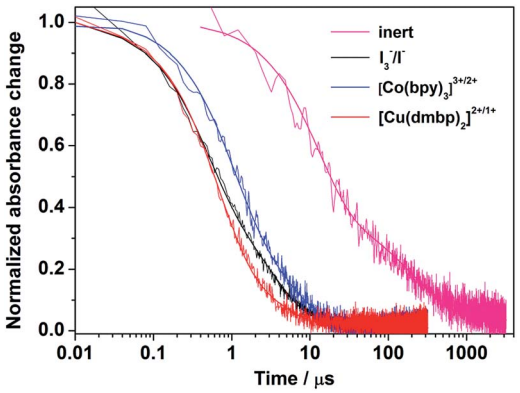

Fig. 4 Transient absorption decay kinetics of the oxidation state of dye **Y123** adsorbed on the TiO_2 film based on the inert and I_3^-/I^-, $[Co(bpy)_3]^{3+/2+}$ and $[Cu(dmbp)_2]^{2+/1+}$ containing electrolytes.

regeneration is extremely low in this $[Cu(dmbp)_2]^{2+/1+}$ system. The HOMO level of organic dye, **Y123**, determined by cyclic voltammetry (Fig. 3(c)) was 1.08 V *vs.* NHE, such that the driving force was merely 0.11 eV (Fig. 3(a)) for dye regeneration. However, the $[Cu(dmbp)_2]^{2+/1+}$ system still has a sufficient dye regeneration speed and rate (details can be found hereinafter). Therefore, the $[Cu(dmbp)_2]^{2+/1+}$ system effectively reduces the energy loss in the dye regeneration process, which leads to an extremely high V_{OC} and yields a remarkable PCE.

The incident photon-to-current conversion efficiency (IPCE) spectra of DSSCs are shown in Fig. 2(b). The IPCE of DSSCs with $[Cu(dmbp)_2]^{2+/1+}$ was more than 80% in the 440–580 nm range with a maximum IPCE above 90% at 520 nm. The remarkable IPCE response for $[Cu(dmbp)_2]^{2+/1+}$ revealed the efficient charge generation, transport, and collection processes in the DSSCs. The UV-vis absorption spectrum of $Cu(dmbp)_2$ BF_4 and $Cu(dmbp)_2(BF_4)_2$ in acetonitrile as well as $[Cu(dmbp)_2]^{2+/1+}$-based dilute electrolyte are shown in Fig. S1† and the corresponding data are listed in Table S1.† The $Cu(dmbp)_2BF_4$ system exhibited an absorption spectrum in 400–500 nm (λ_{max} = 452 nm, ε = 3554 M^{-1} cm^{-1}), whereas the $Cu(dmbp)_2(BF_4)_2$ system showed a maximum absorption at 726 nm in the visible light region with a very low ε of 213 M^{-1} cm^{-1}. As a result, the dilute $[Cu(dmbp)_2]^{2+/1+}$-based electrolyte presents an undesirable absorption spectrum with a maximum absorption at 453 nm (ε = 2281 M^{-1} cm^{-1}), which is competitive with the absorption of the sensitizer on the TiO_2 film. This is the main reason for the lower IPCE values of DSSCs with $[Cu(dmbp)_2]^{2+/1+}$ in the 400–500 nm range. This is also a major argument of the lower J_{SC} for the device with the $[Cu(dmbp)_2]^{2+/1+}$ shuttle.

Transient absorption spectroscopy (TAS) was performed to explore the regeneration dynamics of the oxidation state of **Y123** dye with different redox shuttles. The laser excitation wavelength was at 532 nm and transient absorption changes were monitored at 720 nm. The transient absorption kinetics is exhibited in Fig. 4. The absorption decay of the inert electrolyte with 0.1 M $LiBF_4$ and 0.5 M TBP in acetonitrile shows a half-time ($t_{1/2}$) of 17.2 μs, implying the recombination dynamics of the injected electrons in the TiO_2 conduction band with the oxidation state of dyes. The fast decay dynamics in I_3^-/I^-, $[Co(bpy)_3]^{3+/2+}$, and $[Cu(dmbp)_2]^{2+/1+}$ based electrolytes presented an efficient regeneration of the oxidation state of dyes. The $t_{1/2}$ values of the I_3^-/I^- and $[Cu(dmbp)_2]^{2+/1+}$-based electrolytes were 0.64 μs and 0.60 μs, respectively, which are about two times more than that of the $[Co(bpy)_3]^{3+/2+}$ based electrolyte ($t_{1/2}$ = 1.16 μs). The results demonstrate an efficient regeneration dynamic between the $Cu(dmbp)_2^+$ complex with the oxidation state of the organic dye **Y123**, which is comparable to the I_3^-/I^- system, but much faster than that of the $[Co(bpy)_3]^{3+/2+}$ system. Although the driving force of the device based on $[Cu(dmbp)_2]^{2+/1+}$ is extremely small, the regeneration is still efficient, which can be ascribed to the fast self-exchange from $Cu(dmbp)_2^+$ to $Cu(dmbp)_2^{2+}$.[22,24,25,27] As a result, the energy loss for dye regeneration has been successfully reduced in the $[Cu(dmbp)_2]^{2+/1+}$ system. The regeneration efficiency (ϕ_{Reg}) can be defined as follows (eqn (2)):

$$\phi_{reg} = \frac{k_{reg}}{k_{reg} + k_{rec}} \approx 1 - \frac{t_{1/2,redox}}{t_{1/2,insert}} \quad (2)$$

where k_{reg} is the first-order rate constant of the oxidation state of dye regeneration and k_{rec} is the rate constant of recombination. All three redox systems exhibited high regeneration efficiency over 90%. The ϕ_{reg} of $[Cu(dmbp)_2]^{2+/1+}$ system is 96.5%, which is similar to I_3^-/I^- (ϕ_{reg} = 96.3%) and about 3% higher than that of the $[Co(bpy)_3]^{3+/2+}$ (ϕ_{reg} = 93.3%). The fast regeneration as well as the high regeneration efficiency of $[Cu(dmbp)_2]^{2+/1+}$ provide the device with this redox shuttle a considerable J_{SC}.

Electrochemical impedance spectroscopy (EIS) was performed to elucidate the charge transfer processes of the DSSCs based on three different redox systems. As shown in the Nyquist plots of DSSCs obtained at the same current of 1.35 mA (Fig. S2, ESI†), the left and middle semicircles stand for the charge-transfer resistance at the electrolyte/counter electrode interface (R_{ce}) and dye/TiO_2/electrolyte interface (R_{rec}), respectively. However, the distinct right semicircles for $[Co(bpy)_3]^{3+/2+}$ and $[Cu(dmbp)_2]^{2+/1+}$ systems represent the diffusion resistance of the redox shuttles in the electrolytes. It is obvious that the device with $[Cu(dmbp)_2]^{2+/1+}$ based electrolyte shows the highest R_{ce} among the three redox systems, which can be attributed to two reasons: one is the abovementioned relatively low reduction rate for the $[Cu(dmbp)_2]^{2+/1+}$ system[25] and the other is

the inefficient catalytic activity between platinum and this copper complex shuttle at the counter electrode.[24] Both reasons result in a lower FF. The $[Cu(dmbp)_2]^{2+/1+}$ based DSSC shows a better diffusion process than that of $[Co(bpy)_3]^{3+/2+}$ with a high probability of the smaller molecular size of the copper complexes. There is no large difference in the charge recombination resistance according to the EIS spectra. The $[Cu(dmbp)_2]^{2+/1+}$ system showed a similar resistance to the $[Co(bpy)_3]^{3+/2+}$ system at TiO_2/dye/electrolyte interface, which is slightly smaller than that of I_3^-/I^-. The dark currents of the DSSCs with I_3^-/I^-, $[Co(bpy)_3]^{3+/2+}$, and $[Cu(dmbp)_2]^{2+/1+}$ redox shuttles measured by EIS are shown in Fig. S3 of the ESI.† The higher dark current near 0 V implies more rapid charge recombination from the FTO substrate for the $[Cu(dmbp)_2]^{2+/1+}$ system compared to that of the $[Co(bpy)_3]^{3+/2+}$ and I_3^-/I^- systems.[13,28] The high recombination may result in a low IPCE value, however, this recombination can be reduced by the fast regeneration process between $Cu(dmbp)_2^+$ and the oxidized sensitizer. Hence, the 5–10% decrease in the IPCE value in the region of 420–480 nm with the $[Cu(dmbp)_2]^{2+/1+}$ based device is mainly due to the light absorption. The ~4% decrease in the IPCE value for $[Cu(dmbp)_2]^{2+/1+}$ from the I_3^-/I^- system and the slight decrease of 1–2% from the $[Co(bpy)_3]^{3+/2+}$ system in 500–680 nm is a synthetic result of the electron injection, dye regeneration, and charge collection processes.

Stability tests show that the $[Cu(dmbp)_2]^{2+/1+}$-based devices exhibit a relative stability with a drop of about 10% in PCE for 15 days mainly because of the evaporation of AN under dark conditions. A distinct decrease in PCE with light exposure occurred, which can be attributed to the light-induced ligand exchange (Fig. S4†). Further study of the mechanism of stability with electrolyte and DSSCs will be conducted in the future.

Conclusions

In summary, a [copper(6,6′-dimethyl-2,2′-bipyridine)$_2$]$^{2+/1+}$ redox couple was successfully developed and applied to DSSCs. In combination with an organic sensitizer **Y123**, the $[Cu(dmbp)_2]^{2+/1+}$ system achieved a surprisingly high V_{OC} of 1048 mV, which is 324 mV and 204 mV higher than that of the I_3^-/I^- and $[Co(bpy)_3]^{3+/2+}$ systems. The high V_{OC} can be attributed to the high redox potential of $[Cu(dmbp)_2]^{2+/1+}$. The $[Cu(dmbp)_2]^{2+/1+}$ system showed an extremely low driving force of only 0.11 eV. Moreover, rapid dye regeneration was observed. The dye regeneration process of the $[Cu(dmbp)_2]^{2+/1+}$ system was similar to that of the I_3^-/I^- system, which is two times faster than that of the $[Co(bpy)_3]^{3+/2+}$ system. The low driving force, together with the efficient dye regeneration, remarkably reduced the energy loss in the dye regeneration process of DSSCs. Therefore, an impressive V_{OC} of 1048 mV and an overall efficiency of 10.3% at 100 mW cm^{-2} were achieved. Further enhancements could be expected for this new redox system with broad-spectrum sensitizers, effectively curbed recombination processes and/or optimal counter electrodes. The encouraging results accomplished by the $[Cu(dmbp)_2]^{2+/1+}$ system will definitely shed interesting light on identifying new alternative copper complex-based redox shuttles for the highly efficient DSSCs in the future.

Acknowledgements

We gratefully acknowledge the financial support by China Natural Science Foundation (Grant 21276044, 21606039, 21120102036, 91233201, 51661135021) and the National Basic Research Program of China (Grant No. 2014CB239402).

Notes and references

1 B. O'Regan and M. Grätzel, *Nature*, 1991, **353**, 737.
2 A. Hagfeldt, G. Boschloo, L. Sun, L. Kloo and H. Pettersson, *Chem. Rev.*, 2010, **110**, 6595.
3 H. J. Snaith, *Adv. Funct. Mater.*, 2010, **20**, 13.
4 M. K. Nazeeruddin, A. Kay, I. Rodicio, R. Humphry-Baker, E. Mueller, P. Liska, N. Vlachopoulos and M. Graetzel, *J. Am. Chem. Soc.*, 1993, **115**, 6382.
5 T. W. Hamann and J. W. Ondersma, *Energy Environ. Sci.*, 2011, **4**, 370.
6 Y. Xie, Y. Tang, W. Wu, Y. Wang, J. Liu, X. Li, H. Tian and W. H. Zhu, *J. Am. Chem. Soc.*, 2015, **137**, 14055.
7 G. Boschloo and A. Hagfeldt, *Acc. Chem. Res.*, 2009, **42**, 1819.
8 Z. Zhang, P. Chen, T. N. Murakami, S. M. Zakeeruddin and M. Grätzel, *Adv. Funct. Mater.*, 2008, **18**, 341.
9 S. M. Feldt, E. A. Gibson, E. Gabrielsson, L. Sun, G. Boschloo and A. Hagfeldt, *J. Am. Chem. Soc.*, 2010, **132**, 16714.
10 S. M. Feldt, G. Wang, G. Boschloo and A. Hagfeldt, *J. Phys. Chem. C*, 2011, **115**, 21500.
11 J. Cong, X. Yang, L. Kloo and L. Sun, *Energy Environ. Sci.*, 2012, **5**, 9180.
12 Z. Yu, H. Tian, E. Gabrielsson, G. Boschloo, M. Gorlov, L. Sun and L. Kloo, *RSC Adv.*, 2012, **2**, 1083.
13 J. H. Yum, E. Baranoff, F. Kessler, T. Moehl, S. Ahmad, T. Bessho, A. Marchioro, E. Ghadiri, J. E. Moser, C. Yi, M. K. Nazeeruddin and M. Grätzel, *Nat. Commun.*, 2012, **3**, 631.
14 Z. Yao, M. Zhang, H. Wu, L. Yang, R. Li and P. Wang, *J. Am. Chem. Soc.*, 2015, **137**, 3799.
15 A. Yella, H.-W. Lee, H. N. Tsao, C. Yi, A. K. Chandiran, M. K. Nazeeruddin, E. W.-G. Diau, C.-Y. Yeh, S. M. Zakeeruddin and M. Grätzel, *Science*, 2011, **334**, 629.
16 Z. Yao, H. Wu, Y. Li, J. Wang, J. Zhang, M. Zhang, Y. Guo and P. Wang, *Energy Environ. Sci.*, 2015, **8**, 3192.
17 Z. Yao, M. Zhang, R. Li, L. Yang, Y. Qiao and P. Wang, *Angew. Chem.*, 2015, **54**, 5994.
18 M. Liberatore, A. Petrocco, F. Caprioli, C. La Mesa, F. Decker and C. A. Bignozzi, *Electrochim. Acta*, 2010, **55**, 4025.
19 Z. Sun, M. Liang and J. Chen, *Acc. Chem. Res.*, 2015, **48**, 1541.
20 S. Hattori, Y. Wada, S. Yanagida and S. Fukuzumi, *J. Am. Chem. Soc.*, 2005, **127**, 9648.
21 Y. Bai, Q. Yu, N. Cai, Y. Wang, M. Zhang and P. Wang, *Chem. Commun.*, 2011, **47**, 4376.
22 M. Freitag, F. Giordano, W. Yang, M. Pazoki, Y. Hao, B. Zietz, M. Grätzel, A. Hagfeldt and G. Boschloo, *J. Phys. Chem. C*, 2016, **120**, 9595.

23 During our submission process we found that a similar work was reported in 17 Oct 2016. However, it did not compare the cobalt-complex and iodine system: Y. Saygili, M. Soderberg, N. Pellet, F. Giordano, Y. Cao, A. B. Munoz-Garcia, S. M. Zakeeruddin, N. Vlachopoulos, M. Pavone, G. Boschloo, L. Kavan, J. E. Moser, M. Grätzel, A. Hagfeldt and M. Freitag, *J. Am. Chem. Soc.*, 2016, **138**, 15087–15096.

24 J. Cong, D. Kinschel, Q. Daniel, M. Safdari, E. Gabrielsson, H. Chen, P. H. Svensson, L. Sun and L. Kloo, *J. Mater. Chem. A*, 2016, **4**, 14550.

25 N. Koshino, Y. Kuchiyama, S. Funahashi and H. D. Takagi, *Can. J. Chem.*, 1999, **77**, 1498.

26 H. N. Tsao, C. Yi, T. Moehl, J. H. Yum, S. M. Zakeeruddin, M. K. Nazeeruddin and M. Grätzel, *ChemSusChem*, 2011, **4**, 591.

27 M. Freitag, Q. Daniel, M. Pazoki, K. Sveinbjörnsson, J. Zhang, L. Sun, A. Hagfeldt and G. Boschloo, *Energy Environ. Sci.*, 2015, **8**, 2634.

28 J.-H. Yum, T. Moehl, J. Yoon, A. K. Chandiran, F. Kessler, P. Gratia and M. Grätzel, *J. Phys. Chem. C*, 2014, **118**, 16799.